Earth, Planets and Space

EXPRESS LETTER

Open Access

Reconstructing surface eruptive sequence of 2018 small phreatic eruption of Iwo-yama volcano, Kirishima Volcanic Complex, Japan, by infrasound cross-correlation analysis

Dan Muramatsu[1*], Takeshi Matsushima[2] and Mie Ichihara[3]

Abstract

The Iwo-yama volcano of the Kirishima Volcanic Complex in Japan had a small phreatic eruption in April 2018, which newly formed multiple vents. The activity was recorded by two infrasound sensors and two monitoring cameras, which had been installed within 1 km of the vents. This study identified infrasonic signals from the multiple vents by a cross-correlation analysis between the two infrasound sensors. The analysis successfully revealed the signals from two main eruption craters and constrained the infrasound onsets at the individual vents in the two craters. We combined the infrasound results with the images from the cameras and reconstructed the sequence of the small phreatic eruption of Iwo-yama. At each of the two craters, the intense eruption, which was depicted by the evident infrasound signals, occurred several hours after the eruption onset. This study provides a sequence of the activities of the multiple vents in a phreatic eruption, which will be useful for understanding the phreatic eruption and hazard assessments.

Keywords: Volcano infrasound, Phreatic eruption, Multiple-vent activities, Cross-correlation analysis, Iwo-yama volcano, Monitoring

Introduction

Diverse volcanic activities may produce low-frequency acoustic waves, which are often inaudible to humans. Acoustic waves below 20 Hz are called infrasound. Infrasound observation is a widely used technique to capture surface phenomena associated with various volcanic activities (i.e., Fee and Matoza 2013). Some examples have targeted strombolian eruptions (Vergniolle and Brandeis 1996; Delle Donne and Ripepe 2012; Ishii et al. 2019), vulcanian eruptions (Yokoo et al. 2009; Anderson et al. 2018), subplinian–plinian eruptions (Matoza et al. 2009; Fee et al. 2010), hawaiian eruptions and lava lake activity (Garcés et al. 2003; Bouche et al. 2010), eruption columns (Yamada et al. 2017, 2018; Perttu et al. 2020), and pyroclastic flows (Yamasato 1997; Ripepe et al. 2010). An effective and common method to investigate the infrasonic source location is using an array, which is composed of more than three sensors. This enables signal beamforming for the discrimination of different activities at multiple vents. It also helps distinguish volcanic signals from uncorrelated noise or infrasound from non-volcanic sources (Ripepe and Marchetti 2002; Johnson and Ripepe 2011; Yamakawa et al. 2018; Matoza et al. 2019). However, the construction and maintenance of arrays in volcanic regions is not easy, and only a few volcanoes are equipped with permanent infrasound arrays. Although infrasound detection methods using a single infrasound microphone and a collocated seismometer have been proposed (Ichihara et al. 2012; McKee et al. 2018), they may not be applicable when a volcano is seismically very

*Correspondence: muramatsu@sevo.kyushu-u.ac.jp
[1] Department of Earth and Planetary Sciences, Graduate School of Science, Kyushu University, 744 Motooka, Nishi-ku, Fukuoka 819-0395, Japan
Full list of author information is available at the end of the article

active. Alternatively, using a pair of microphones significantly improves infrasound detection over a single sensor (Castaño et al. 2020) and helps to estimate source locations (Walsh et al. 2019).

During phreatic eruptions, multiple vents are frequently formed one after another at the ground surface (e.g., Yukutake et al. 2017; Mannen et al. 2018). Identifying multiple-vent activities is essential for understanding the transition process of phreatic eruptions and hazard assessments. The 2018 eruption of the Iwo-yama volcano of the Kirishima Volcanic Complex (KVC) in Japan is a case of phreatic eruptions with successive vent formations. Two infrasonic sensors and monitoring cameras recorded the events within 1 km of the newly formed vents. In this study, we performed acoustic cross-correlation analyses between the two infrasound sensors to reveal the activities of the individual vents. We also referred to the monitoring images and then, reconstructed the sequence of the small phreatic eruption at the Iwo-yama volcano.

Data

Infrasonic data

Infrasonic data were collected at KU.EBQ7 station, 387 m southwest of the summit of Iwo-yama, and KU.KREB station, 842 m west of the summit (Fig. 1a). The average distances from the 2018 eruption vents (red circles in Fig. 1a) to KU.EBQ7 and KU.KREB were 214 m and 556 m, respectively. Infrasound was recorded using a Hakusan SI104 microphone (Hakusan Corporation, Japan) at KU.EBQ7 (hereafter referred to as MC1) at 200-Hz sampling frequency and a Hakusan SI102 microphone at KU.KREB (MC2) at 100 Hz. Both microphones have flat responses in a frequency range above 0.05 Hz. The time-series data were logged continuously with a 24-bit resolution by an HKS-9700 logger (Keisokugiken Corporation, Japan) at KU.EBQ7 and an LS-7000XT logger (Hakusan Corporation, Japan) at KU.KREB.

Monitoring camera

Monitoring camera data were provided by the Kagoshima Local Meteorological Office of the Japan Meteorological Agency (JMA). There were two video cameras around Iwo-yama volcano. The Iwo-yama–Minami monitoring camera (CAM1) was located 204 m to the south of the summit, and the Ebinokogen monitoring camera (CAM2) was located 930 m to the west (Fig. 1a). The average distances from the vents to CAM1 and CAM2 were 347 m and 617 m, respectively. Because these are visible light cameras, the phreatic eruption clouds were not visible at night. The sampling rate was approximately 6 s. The vents were formed in front of either one of the cameras, and therefore, their activities were successfully captured during the daytime.

Overview of the 2018 small phreatic eruption of Iwo-yama

KVC is composed of ~ 20 volcanoes and is located in the southern part of Kyushu Island, Japan (Fig. 1a). One of the active cones of KVC is Iwo-yama, which has subsurface hydrothermal systems and surface geothermal activities (Tsukamoto et al. 2018). From April 19–21, 2018, a small phreatic eruption occurred at Iwo-yama and opened multiple new vents outside of the existing craters ('Old craters' in Fig. 1b). The vents emitted ash–steam mixtures up to 500 m. During this eruption, infrasonic signals were recorded by the observation sites near the vents (Fig. 1a). The eruptive activity was localized in two areas, which were the Iwo-yama South Craters (hereafter, the South Crater), consisting of several sub-craters, and Iwo-yama West Crater (hereafter, the West Crater) (Tajima et al. 2020). The craters were composed of several vents, namely S1 to S7 in the South Crater and W1 to W7 in the West Crater (Fig. 1b). The eruption began with the formation of the new vents S1 and S5 in the South Crater from April 19, 2018, at 15:39 JST (all times hereafter are in Japan Standard Time), and the other vents were subsequently formed and merged into three sub-craters (Tajima et al. 2019). These were vents S1–S3 to the sub-crater Y3, S4–S6 to Y2a, and S7 to Y2b (Fig. 1b). Hereafter, we call these three sub-craters (Y2a, Y2b, and Y3) as vents because our analysis does not have resolutions to discriminate individual vents (S1–S7) in the South Crater. At approximately 16:30 on April 20, steaming began 500 m to the west of the South Crater, and the new vents (W1–W7) were formed before the morning of April 21. The vents W3 and W4 grew to a crater, around which ashy deposits and ejecta were observed. It is considered that the ejection occurred in the evening of April 20 (Tajima et al. 2020). After the eruption, vigorous fumarolic activity and hot water swelling from the vents persisted for over a year.

Figure 2 shows the waveform and spectrogram of the infrasound recorded by MC2, and the snapshots taken by the monitoring cameras that captured surface phenomena at the two crater areas. During the entire period from 15:00 on April 19 to 7:00 on April 21 (Fig. 2a, b), tremor-like infrasound, with an amplitude of up to ~ 1 Pa at KU.KREB (~ 800 m from the South Crater) consisting of two frequency bands, 1–7 Hz and 7–20 Hz, was observed. The eruption onset in the South Crater was clearly captured by CAM1 (Fig. 2c, d) and was recognized by the sudden increase in the infrasound amplitude (Fig. 2a,b). The West Crater area was recorded by CAM2, where faint fumaroles began rising at approximately 16:30 on April 20 (Fig. 2e, f). However, the time

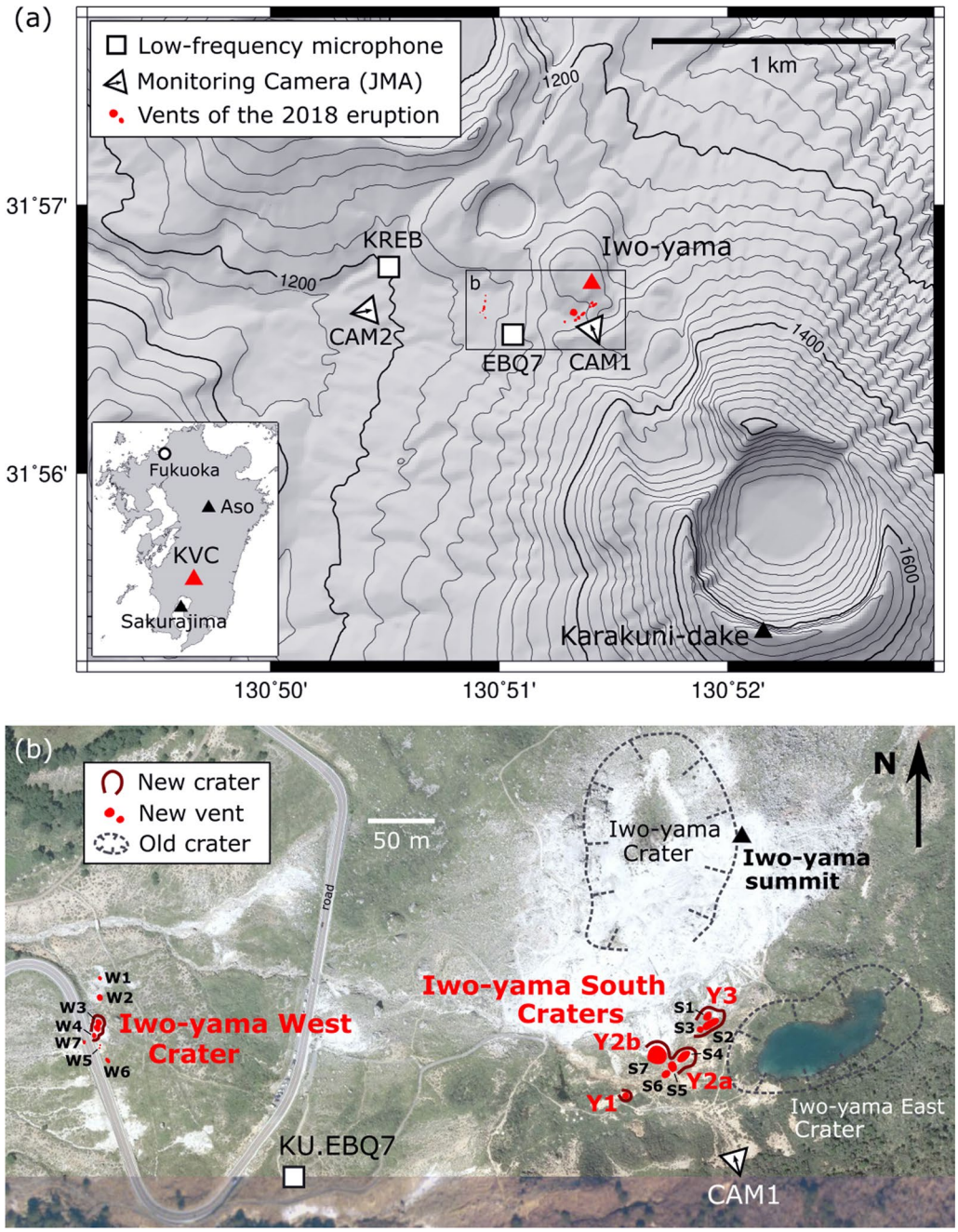

Fig. 1 Observation sites and crater locations. **a** Iwo-yama volcano (summit is indicated by the red triangle) and the locations of the observation sites. The contour interval is 20 m. The small red circles are the vents of the 2018 small phreatic eruption. The region surrounded by the rectangle is enlarged in **b**. Map inset shows the location of Kirishima Volcanic Complex (KVC) on Kyushu Island, southwest of Japan. **b** Craters and vents of the 2018 eruption. Their locations and naming were cited from Tajima et al. (2020). The photograph was taken from GSI Tiles, of the Geospatial Information Authority of Japan. There are two newly formed main craters, Iwo-yama South Craters (the South Crater) and Iwo-yama West Crater (the West Crater). The craters were composed of several vents, namely S1 to S7 in the South Crater and W1 to W7 in the West Crater. After the onset of the eruption, the vents in the South Crater merged into three sub-craters (Y2a, Y2b, and Y3); the vents S1–S3 to Y3, S4–S6 to Y2a, and S7 to Y2b. In this study, we call the sub-craters as vents because our analysis does not have a resolution to discriminate the individual vents in the South Crater (S1–S7). Y1 appeared on April 7, 12 days before the eruption. We excluded it from the discussion because it did not participate in the eruption

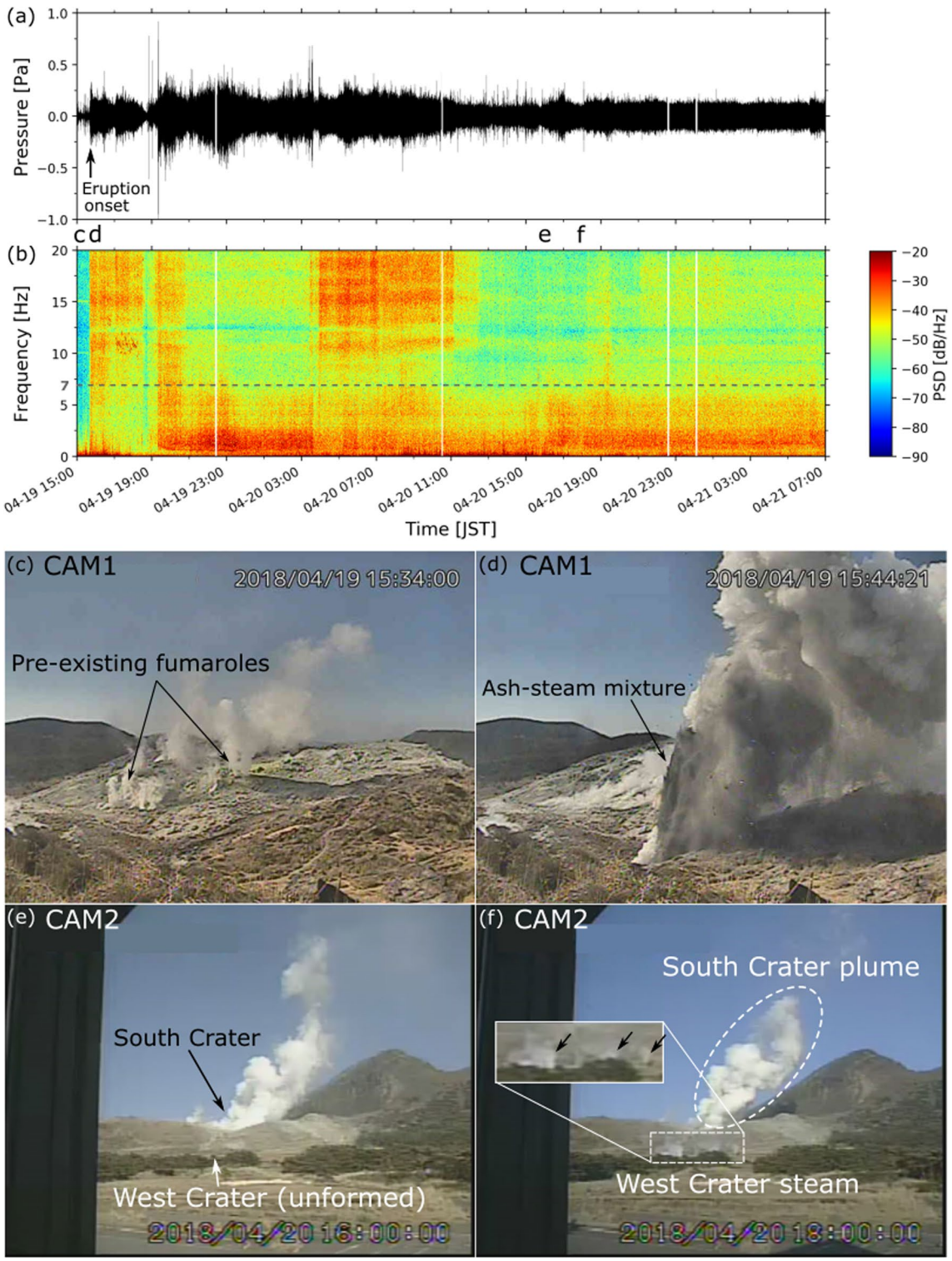

Fig. 2 Waveform and spectrogram of infrasound recorded by MC2 and the snapshots that captured surface phenomena associated with the eruption by CAM1 and CAM2. **a** Infrasound waveform filtered 0.3–20 Hz. The vertical white lines represent data-missing periods due to equipment problems. **b** Spectrogram of the nonfiltered infrasonic signal calculated using 10.24-s sliding windows with 50% overlaps. We observed infrasonic powers in two frequency bands separated at 7 Hz (gray dashed line). The middle panels show snapshots of the South Craters taken by CAM1 just prior to the eruption (**c**) and at the onset of the eruption (**d**). The bottom panels are snapshots taken by CAM2 that show the West Crater before the eruption (**e**) and emitting faint steam, which indicated by black arrows (**f**)

of the small eruption from vents W3 and W4 could not be confirmed with the monitoring camera recordings as it occurred at night. We aim to distinguish the acoustic signals of the West Crater from those of the South Crater.

Method

Cross-correlation analysis

We conducted an acoustic cross-correlation analysis (e.g., Garcés et al. 2003; Scott et al. 2007; Johnson and Palma 2015; Walsh et al. 2019) between two microphones, MC1 (KU.EBQ7) and MC2 (KU.KREB); the distance between MC1 and MC2 is 585 m. Walsh et al. (2019) used a similar method for analyzing pulse events in the phreatic eruption of White Island, New Zealand. They showed that the lag time of infrasound obtained by a cross-correlation analysis was consistent with the eruption vent locations inferred from the amplitude distributions of the corresponding seismic pulses and concluded that the eruption signals originated from a single vent, but from varying depths in the vent. In this study, we attempted to distinguish the tremor-like infrasound signals from multiple vents referring to visual observations.

We investigated the temporal change of the cross-correlation coefficient $R(t,\tau) = R[\tau; P_1(t,x_1), P_2(t,x_2)]$, where P_1 and P_2 are the acoustic signals recorded at points x_1 and x_2, respectively, and τ is the lag time of P_1 to P_2. We calculated $R(t,\tau)$ using time windows of a fixed length of 5 s starting at t and incorporating 60% overlaps. The result is graphically displayed on the $t-\tau$ axis. The function $R(t,\tau)$ has a peak at a particular lag time that corresponds to the acoustic travel time difference between the two observation points when a coherent acoustic signal exists. Depending on the signal's lag time and spectral features, the $t-\tau$ plot has a characteristic pattern that aids signal identification. Since we observed infrasonic powers in two frequency bands separated at 7 Hz in the spectrogram (Fig. 2b), we performed the correlation analyses in two frequency bands, 1–7 and 7–20 Hz.

Estimation of expected lag time

Herein, the candidate source locations (the new vents in the South Crater and the West Crater) are known, and therefore, the expected lag times are estimated. For simplicity, we assumed linear and isotropic propagation for acoustic waves. The expected lag time was then calculated as $(d_1 - d_2)/c$, where d_1 and d_2 are the travel distances of the signal from the source to the observation points x_1 and x_2, respectively, and c is the atmospheric sound speed. The atmospheric sound speed is calculated by assuming an ideal gas, $c = \sqrt{\gamma R_g T}$, where γ is the heat capacity ratio (1.4), R_g is the gas constant of air (287 J/kg/K), and T is the atmospheric temperature in K (Landau and Lifshitz 1987). The atmospheric temperature fluctuates with time, and the wind speed and direction also affect the sound propagation velocity (Garcés et al. 1998). As the low-frequency infrasound noise increases with wind speed (Woodward et al. 2005), the infrasound noise level in our data suggests that the wind was weak, though a meteorological station was not present around Iwo-yama. Therefore, we ignored the wind effect and calculated the theoretical temperature at an altitude of 1300 m from hourly temperature data collected at the Kakuto station (228 m a.s.l.) of JMA, which is the closest meteorological observation site (~12 km from Iwo-yama). The estimated atmospheric temperature ranged from 272–296 K, and the resultant sound speed ranged from 330.7–345.0 m/s during the period from 15:00 on April 19 to 7:00 on April 21. Using these values, we estimated the possible ranges of the expected lag times. Assuming the sources in the South Crater at Y2a, Y2b, and Y3, the expected lag times are 1.46–1.57 s. If the source vents are located in the West Crater (W3 and W4), the expected lag times are 0.70–0.74 s. The values for all the vents and craters are shown in Additional file 1: Table S1.

Results and discussion

Figure 3 shows the results of the cross-correlation analysis. The top panel (Fig. 3a) shows the waveforms filtered at 1–7 Hz and 7–20 Hz. The middle and bottom panels show $t-\tau$ plots of the cross-correlation coefficient in the frequency ranges of 1–7 Hz (Fig. 3b) and 7–20 Hz (Fig. 3c), both of which exhibit high correlation values around $\tau = 1.5$ s after 15:39:45 on April 19. This lag time is equivalent to that expected for infrasound from the South Crater, which confirms that its eruptive activity persisted over the analyzed period after the onset. The correlation values in the lower-frequency band increase at 19:19:40 (Fig. 3b), coincident with the amplitude increase (Fig. 3a). Simultaneously, CAM1 captured the widening of the Y2a vent, which began at 18:40:51, with increased ash plumes from the vent (Additional file 2: Fig. S1). We consider that an intense eruption, accompanying the infrasonic signals dominated by the low-frequency (1–7 Hz) band, began at 19:19:40 after the vent widening. From around 3:57 on April 20, the correlation values around $\tau = 1.5$ s in the higher-frequency band intensified again (Fig. 3c). Besides, subtle peaks in $\tau < 0.9$ s, indicating the West Crater signals, appear around 21:00 on April 20 in the 7–20 Hz band; however, the correlation pattern is unclear to constrain the onset (Fig. 3c).

We improved the resolution using the following procedure: The data were resampled up to 500 Hz by linear interpolation to increase the lag time resolution. We then calculated the cross-correlation coefficients for 5-s-long

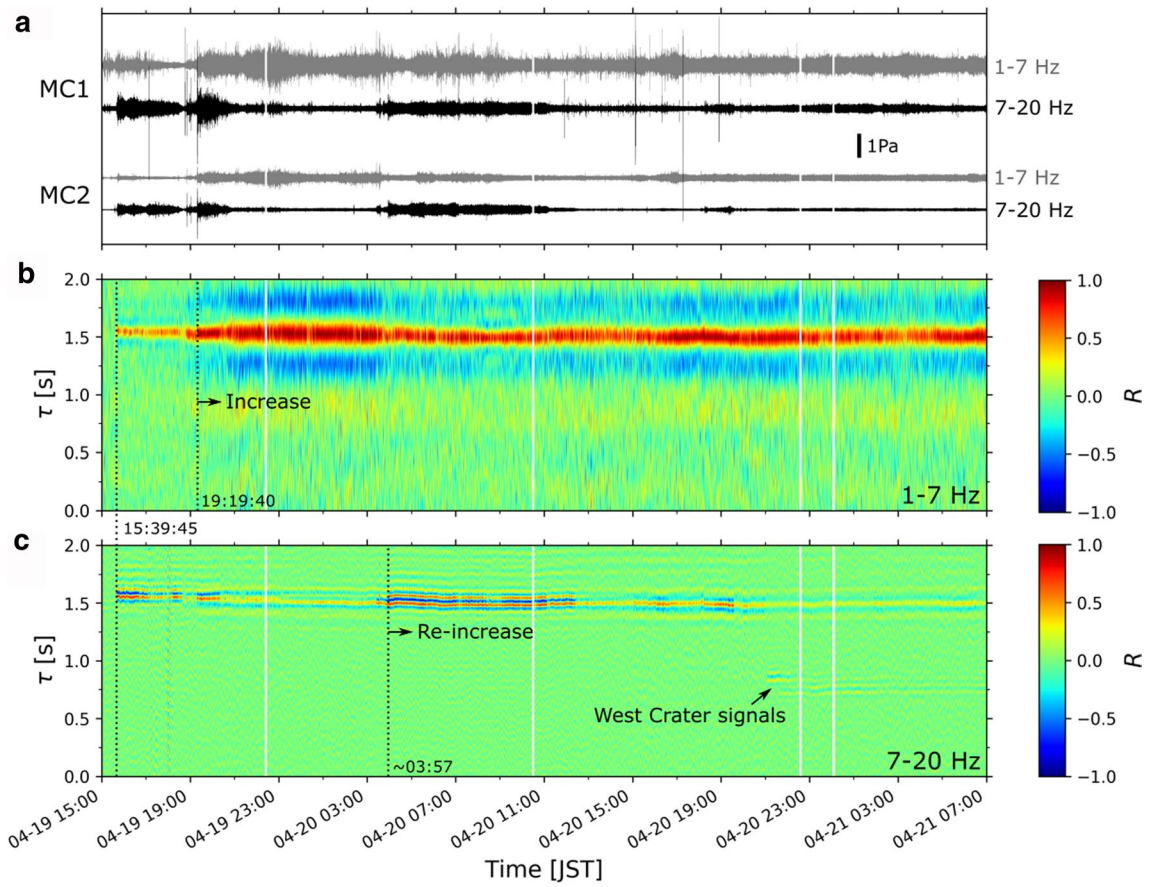

Fig. 3 Cross-correlation analysis between MC1 and MC2. The vertical white lines represent periods with missing data. **a** Waveforms filtered 1–7 Hz (gray lines) and 7–20 Hz (black lines) recorded by MC1 and MC2. **b** The $t - \tau$ plot of the cross-correlation coefficient in the frequency range of 1–7 Hz. The signal starts with the eruption onset at 15:39:45 on April 19, and the correlation values increase from 19:19:40 on April 19 (black dotted line). **c** The cross-correlation coefficient in the frequency range of 7–20 Hz. The correlation peaks appear with the eruption onset and re-intensify after around 3:57 on April 20 (black dotted line)

time windows sliding in 2 s, and progressively stacked them every 20 s. The results for the higher-frequency band are shown in Fig. 4, and the results for the lower-frequency band are provided in Additional file 3.

By analyzing the South Crater signals, the lag time of the initial stage of the eruption is 1.55 s, whereas that after the reincrease (3:57 on April 20) is 1.50 s. (Fig. 4b). Referring to the expected lag times of the South Crater signals (Table S1), we consider that the shortening of the correlation peak lag time by 0.05 s indicates the source shift from Y2a to Y3. The lag time starts shortening simultaneously with the vent widening at 18:40:51, and before the low-frequency power increase at 19:19:40 (Fig. 3b). The images from CAM1 also show increased ash plumes from Y3 with the widening of Y2a (Additional file 2: Fig. S1). We interpret that Y3 was activated with the vent widening and then, from around 3:57 on April 20, became the main source of the higher-frequency infrasonic signals.

At the West Crater, there is no clear correlation in the corresponding range τ before 21:00 (Fig. 4c), although CAM2 recorded faint steam clouds from around 16:30. A possible reason is that the signal was below the detection level, or was buried in the strong signal from the South Crater. At $21{:}05{:}20 \pm 10$ s, a correlation peak appears around $\tau = 0.83$ s (Fig. 4c), which corresponds to vent W6 (Additional file 1: Table S1). The correlation decays after 22:00. Another peak then appears around $\tau = 0.72$ s from $21{:}42{:}20 \pm 10$ s (Fig. 4c), which we infer as the onset of the small eruption from vents W3 and W4 that erupted ash and ejecta.

The relationships between the correlation peak time lags and the source positions are subject to uncertainties regarding the atmospheric temperature and the local wind speed. We checked the validity of the interpretations described above in the following. For the South Crater, the peak at $\tau = 1.55$ s is related to Y2a with the atmospheric sound speed and temperature of 336 m/s

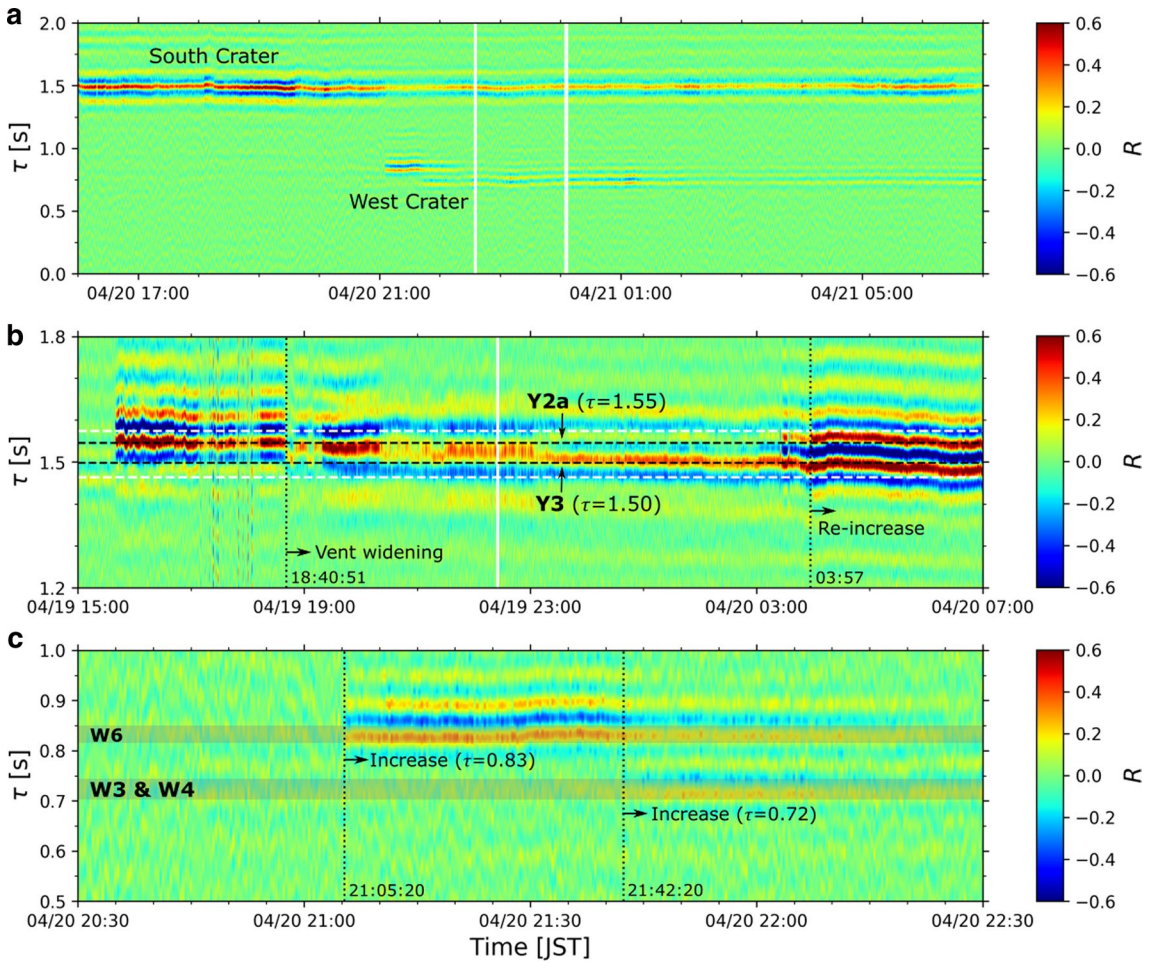

Fig. 4 Stacked cross-correlation coefficients for the higher-frequency band. **a** The $t - \tau$ plot of the stacked cross-correlation coefficients in the frequency range of 7–20 Hz from 16:00 on April 20 to 7:00 on April 21. The vertical white lines represent periods with missing data. **b** The plot focusing on the South Crater signals from 15:00 on April 19 to 7:00 on April 20. The expected lag time ranges of the South Crater (1.46–1.58 s) are bounded by the horizontal white dashed lines. The horizontal black dashed lines are $\tau = 1.55$ s and 1.50 s, corresponding to Y2a and Y3, respectively. The vertical dotted lines mark times of the vent widening onset (18:40:51 on April 19) and emergence of the high-frequency signal power (3:57:00, on April 20). **c** Enlarged view of the $t - \tau$ plot from 20:30 to 22:30 on April 20. Gray shaded regions indicate the expected lag times of the vents W3–W4 and W6. The clear signals appear at 21:05:20 from W6 and at 21:42:20 from W3–W4 (vertical dotted lines)

and 281 K, respectively. If the signal is from Y3, the atmosphere should have 326 m/s and 265 K, respectively. Alternatively, if the peak at $\tau = 1.50$ s is made by Y2a, it requires 347 m/s and 300 K. These values are outside the range of the estimated atmospheric temperature. It is also unrealistic that the temperature increased by nearly 20 K from 16:00 on April 19 to 4:00 on April 20; neither can we assume that the wind speed increased more than 10 m/s when considering the low-frequency noise level of the infrasound data (Fig. 3a). For the West Crater, if the peak at $\tau = 0.83$ s corresponds to W3 and W4 instead of W6, the sound speed and the atmospheric temperature need to be as low as 292 m/s and 212 K, respectively. If the peak at $\tau = 0.72$ s is vent W6, it requires extremely large values of 390 m/s and 379 K. We contend that realistic atmospheric conditions cannot generate such extreme propagation speeds.

We reconstructed the sequence of the multiple-vent activities of the 2018 small phreatic eruption of Iwo-yama and summary our finding in Fig. 5. The South Crater began an eruption at 15:39 on April 19, mainly from Y2a (and Y2b). The vent widened from 18:40 to 19:19, which was followed by an intensification of the eruption accompanied by the lower-frequency infrasonic signals. Vent Y3 was activated with the Y2a widening and became the main source of higher-frequency infrasonic signals from 3:57 on April 20. The steam-emitting vents appeared in the West Crater area around 16:30 on April 20, and the

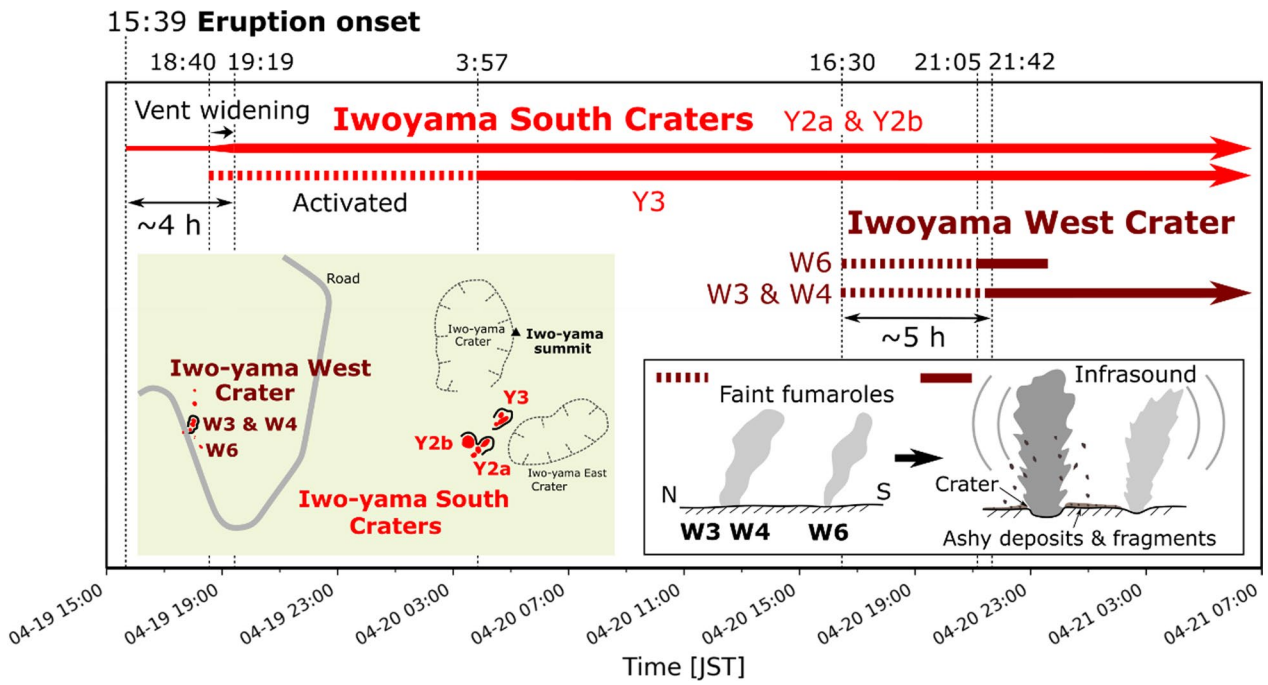

Fig. 5 Summary of the reconstructed sequence of the 2018 small phreatic eruption of Iwo-yama volcano. The eruption began at 15:39 on April 19 at Y2a in the South Crater area. The Y2a vent widened from 18:40, and then the eruption intensified from 19:19. Simultaneously with the vent widening, Y3 was activated and then became the main source of high-frequency infrasonic signals after 3:57 on April 20. Weak fumaroles appeared in the West Crater area around 16:30 on April 20. An eruption or gas emission started from 21:05 at W6. A small eruption emitting ash and ejecta occurred at 21:42 at W3–W4, resulting in the formation of a crater

eruptions accompanying infrasonic signals occurred from 21:05 successively, in multiple vents. These observations suggest that the intense eruptions started with several hours of delay after the onset of steaming or the appearance of the vents.

Several hours of delay in the vent formation accompanying ash falls with intensified seismic tremor after the infrasound onset was also observed in the 2015 small phreatic eruption of the Hakone volcano, Japan (Yukutake et al. 2017). The delay has been interpreted as the time for the hydrothermal fluid to reach the ground surface from a subsurface open-crack source, while the infrasound began concurrently with the crack opening by strain transfer (Yukutake et al. 2018). The time delay between the onset of surface phenomena and the intense eruptions can be a common feature of small-scale phreatic eruptions (e.g., Mannen et al. 2018; Kilgour et al. 2019). Our results add another case and will be useful for considering the mechanism of the transition process of small-scale phreatic eruptions and assessing the hazards of eruptions that form multiple vents.

The intensification of the eruption accompanied by lower-frequency infrasonic signals coincided with the vent widening. For instance, in magmatic eruptions, Fee et al. (2017) suggested the vent widening during a phreatic eruption of Pavlof volcano, which they attributed to the vent erosion by a high-speed gas–particle flow resulting from the explosive fragmentation. However, no evidence indicating such explosive processes was found in the field (Tajima et al. 2020) or in the monitoring camera data during the phreatic eruption of Iwo-yama. We infer that some non-explosive processes caused the vent widening there. For example, interaction with hot water might have weakened the ground surface around the vent to cause subsidence or collapse. Further studies, including seismic data analyses, could identify the widening mechanism, which is beyond the scope of this paper.

We found signals in the two separate frequency bands and interpret their temporal fluctuations as a reflection of the dynamics and transition of the eruptive activity. At the West Crater area, the geological survey found ash deposits and fragments around W3 and W4 (Tajima et al. 2020), but only traces of mud flows from W6 (Tajima et al. 2019). Conversely, the signal from W6 exhibits a clearer correlation than that from W3 and W4 (Fig. 4c), indicating that the former has more significant power. We note that the infrasonic power does not necessarily represent the amount of ash emission. The generation mechanism of infrasound accompanying phreatic eruptions is only partially understood (e.g.,

Jolly et al. 2016), and we plan to investigate the source process of the infrasonic signals at Iwo-yama in future work.

Conclusions

We reconstructed the sequence of the multiple-vent activities of the 2018 small phreatic eruption of the Iwo-yama volcano in Japan by conducting an acoustic cross-correlation analysis between two infrasound sensors. We identified infrasound signals from the South Crater that were associated with the eruption onset and the vent widening that had been observed by the monitoring camera. We also constrained the timing of the significant eruptive activity at the individual vents in both the South Crater and the West Crater during the nighttime, which had not been confirmed visually. The results suggested that the intense eruptions with detectable infrasound began several hours after the onset of steaming or the vents' appearance. In addition, it is observed that intense infrasound does not necessarily accompany a large amount of ash emission, as is the case with W6. Our results demonstrate a case of the transition processes of phreatic eruptions that form multiple vents. These findings will be useful in constraining the mechanism and assessing eruption hazards.

Supplementary Information

The online version contains supplementary material available at https://doi.org/10.1186/s40623-020-01344-6.

Additional file 1. Expected lag times for each crater and vent.

Additional file 2. Eruption onset and vent widening captured by CAM1.

Additional file 3. Correlation peaks of the South Crater in the lower-frequency band.

Abbreviations

KVC: Kirishima Volcanic Complex; JMA: Japan Meteorological Agency; GSI: Geospatial Information Authority of Japan; JST: Japan Standard Time.

Acknowledgements

We thank K. Aizawa and Y. Tajima for their insightful discussions and comments. We thank the Kagoshima Local Meteorological Office, JMA, who provided the monitoring camera data. The aerial photograph used in Fig. 1 was taken from the GSI Tiles of the Geospatial Information Authority of Japan. Constructive comments from two anonymous reviewers and associate editor A. Jolly have greatly improved the manuscript. This work was supported by the MEXT Earthquake and Volcano Hazards Observation and Research Program, MEXT Integrated Program for Next Generation Volcano Research and Human Resource Development, ERI JURP 2016B03, and JSPS KAKENHI Grant Number JP20J10734.

Authors' contributions

DM analyzed the data and drafted the manuscript. TM contributed to the data acquisition and maintaining the observation network. MI supported the analysis and developed the theoretical background. All authors read and approved the final manuscript.

Funding

This work was supported by the MEXT Earthquake and Volcano Hazards Observation and Research Program, MEXT Integrated Program for Next Generation Volcano Research and Human Resource Development, ERI JURP 2016B03, and JSPS KAKENHI Grant Number JP20J10734.

Availability of data and materials

The infrasound data are available from the corresponding author on request. The monitoring camera data belong to the Kagoshima Local Meteorological Office of the Japan Meteorological Agency, so please contact them.

Ethics approval and consent to participate

Not applicable

Consent for publication

Not applicable

Competing interests

The authors declare that they have no competing interests.

Author details

[1] Department of Earth and Planetary Sciences, Graduate School of Science, Kyushu University, 744 Motooka, Nishi-ku, Fukuoka 819-0395, Japan. [2] Institute of Seismology and Volcanology, Faculty of Science, Kyushu University, 2-5643-29 Shin'yama, Shimabara 855-0843, Japan. [3] Earthquake Research Institute, University of Tokyo, 1-1-1 Yayoi, Bunkyo-ku, Tokyo 113-0032, Japan.

Received: 30 October 2020 Accepted: 21 December 2020
Published online: 05 January 2021

References

Anderson JF, Johnson JB, Steele AL, Ruiz MC, Brand BD (2018) Diverse eruptive activity revealed by acoustic and electromagnetic observations of the 14 july 2013 intense vulcanian eruption of Tungurahua volcano. Ecuador Geophys Res Lett 45(7):2976–2985. https://doi.org/10.1002/2017GL076419

Bouche E, Vergniolle S, Staudacher T, Nercessian A, Delmont J-C, Frogneux M, Cartault F, Le Pichon A (2010) The role of large bubbles detected from acoustic measurements on the dynamics of Erta'Ale lava lake (Ethiopia). Earth Planet Sci Lett 295(1–2):37–48. https://doi.org/10.1016/j.epsl.2010.03.020

Castaño LM, Ospina CA, Cadena OE, Galvis-Arenas B, Londono JM, Laverde CA, Kaneko T, Ichihara M (2020) Continuous monitoring of the 2015–2018 Nevado del Ruiz activity, Colombia, using satellite infrared images and local infrasound records. Earth, Planets Space https://doi.org/10.1186/s40623-020-01197-z

Delle Donne D, Ripepe M (2012) High-frame rate thermal imagery of strombolian explosions: Implications for explosive and infrasonic source dynamics. J Geophys Res Solid Earth. https://doi.org/10.1029/2011JB008987

Fee D, Garces M, Steffke A (2010) Infrasound from Tungurahua volcano 2006–2008: strombolian to plinian eruptive activity. J Volcanol Geotherm Res 193(1–2):67–81. https://doi.org/10.1016/j.jvolgeores.2010.03.006

Fee D, Haney MM, Matoza RS, Van Eaton AR, Cervelli P, Schneider DJ, Iezzi AM (2017) Volcanic tremor and plume height hysteresis from Pavlof Volcano Alaska. Science 355(6320):45–48. https://doi.org/10.1126/science.aah6108

Fee D, Matoza RS (2013) An overview of volcano infrasound: From Hawaiian to Plinian, local to global. J Volcanol Geotherm Res 249:123–139. https://doi.org/10.1016/j.jvolgeores.2012.09.002

Garcés M, Hansen R, Lindquist K (1998) Traveltimes for infrasonic waves propagating in a stratified atmosphere. Geophys J Int 135(1):255–263. https://doi.org/10.1046/j.1365-246X.1998.00618.x

Garcés M, Harris A, Hetzer C, Johnson J, Rowland S, Marchetti E, Okubo P (2003) Infrasonic tremor observed at Kīlauea Volcano. Hawai'i Geophys Res Lett. https://doi.org/10.1029/2003gl018038

Ichihara M, Takeo M, Yokoo A, Oikawa J, Ohminato T (2012) Monitoring volcanic activity using correlation patterns between infrasound and ground motion. Geophys Res Lett. https://doi.org/10.1029/2011GL050542

Ishii K, Yokoo A, Kagiyama T, Ohkura T, Yoshikawa S, Inoue H (2019) Gas flow dynamics in the conduit of Strombolian explosions inferred from seismo-acoustic observations at Aso volcano, Japan. Earth Planets Space https://doi.org/10.1186/s40623-019-0992-z

Johnson JB, Palma JL (2015) Lahar infrasound associated with Volcán Villarrica's 3 March 2015 eruption. Geophys Res Lett 42(15):6324–6331. https://doi.org/10.1002/2015GL065024

Johnson JB, Ripepe M (2011) Volcano infrasound: a review. J Volcanol Geotherm Res 206(3–4):61–69. https://doi.org/10.1016/j.jvolgeores.2011.06.006

Jolly A, Kennedy B, Edwards M, Jousset P, Scheu B (2016) Infrasound tremor from bubble burst eruptions in the viscous shallow crater lake of White Island, New Zealand, and its implications for interpreting volcanic source processes. J Volcanol Geotherm Res 327:585–603. https://doi.org/10.1016/j.jvolgeores.2016.08.010

Kilgour G, Gates S, Kennedy B, Farquhar A, Mcsporran A, Asher C (2019) Phreatic eruption dynamics derived from deposit analysis: a case study from a small, phreatic eruption from Whakāri/White Island, New Zealand. Earth, Planets Space 71:36. https://doi.org/10.1186/s40623-019-1008-8

Landau L, Lifshitz E (1987) Fluid Mechanics, 2nd edn. Pergamon Press, Oxford

Mannen K, Yukutake Y, Kikugawa G, Harada M, Itadera K, Takenaka J (2018) Chronology of the 2015 eruption of Hakone volcano, Japan: geological background, mechanism of volcanic unrest and disaster mitigation measures during the crisis. Earth, Planets Space https://doi.org/10.1186/s40623-018-0844-2

Matoza RS, Arciniega-Ceballos A, Sanderson RW, Mendo-Pérez G, Rosado-Fuentes A, Chouet BA (2019) High-broadband seismoacoustic signature of vulcanian explosions at popocatépetl volcano. Mexico Geophys Res Lett 46(1):148–157. https://doi.org/10.1029/2018GL080802

Matoza RS, Fee D, Garcés MA, Seiner JM, Ramón PA, Hedlin MAH (2009) Infrasonic jet noise from volcanic eruptions. Geophys Res Lett. https://doi.org/10.1029/2008GL036486

McKee K, Fee D, Haney M, Matoza RS, Lyons J (2018) Infrasound signal detection and back azimuth estimation using ground-coupled airwaves on a seismo-acoustic sensor pair. J Geophys Res Solid Earth 123(8):6826–6844. https://doi.org/10.1029/2017JB015132

Perttu A, Taisne B, De AS, Assink JD, Tailpied D, Williams RA (2020) Estimates of plume height from infrasound for regional volcano monitoring. J Volcanol Geotherm Res. https://doi.org/10.1016/j.jvolgeores.2020.106997

Ripepe M, De Angelis S, Lacanna G, Voight B (2010) Observation of infrasonic and gravity waves at Soufrière Hills Volcano, Montserrat. Geophys Res Lett. https://doi.org/10.1029/2010GL042557

Ripepe M, Marchetti E (2002) Array tracking of infrasonic sources at Stromboli volcano. Geophys Res Lett 29(22):33–41. https://doi.org/10.1029/2002gl015452

Scott E, Hayward C, Kubichek R, Hamann J, Pierre J, Comey B, Mendenhall T (2007) Single and multiple sensor identification of avalanche-generated infrasound. Cold Reg Sci Technol 47(1–2):159–170. https://doi.org/10.1016/j.coldregions.2006.08.005

Tajima Y, Nakada S, Maeno F, Huruzono T, Takahashi M, Inamura A, Matsushima T, Nagai M, Funasaki J (2020) Shallow magmatic hydrothermal eruption in April 2018 on Ebinokogen Ioyama volcano in Kirishima volcano group, Kyushu. Japan Geosciences 10(5):183. https://doi.org/10.3390/geosciences10050183

Tajima Y, Nakada S, Nagai M, Maeno F, Watanabe A (2019) Small eruption at the Ebinokogen Ioyama volcano of the Kirishima Volcano Group in April 2018. Bull Volcanol Soc Japan 64(2):147–151. https://doi.org/10.18940/kazan.64.2_147

Tsukamoto K, Aizawa K, Chiba K, Kanda W, Uyeshima M, Koyama T, Utsugi M, Seki K, Kishita T (2018) Three-dimensional resistivity structure of iwo-yama volcano, kirishima volcanic complex, Japan: relationship to shallow seismicity, surface uplift, and a small phreatic eruption. Geophys Res Lett 45(23):12821–12828. https://doi.org/10.1029/2018GL080202

Vergniolle S, Brandeis G (1996) Strombolian explosions 1. A large bubble breaking at the surface of a lava column as a source of sound. J Geophys Res B Solid Earth 101(9):20433–20447. https://doi.org/10.1029/96jb01178

Walsh B, Procter J, Lokmer I, Thun J, Hurst T, Christenson B, Jolly A (2019) Geophysical examination of the 27 April 2016 Whakaari/White Island, New Zealand, eruption and its implications for vent physiognomies and eruptive dynamics. Earth, Planets Space https://doi.org/10.1186/s40623-019-1003-0

Woodward R, Israelsson H, Bondár I, Mclaughlin K, Bowman JR, Bass H (2005) Understanding wind-generated infrasound noise. Proc. 27th Seism. Res. Rev. Ground-Based Nucl. Explos. Monit. Technol. 866–875

Yamada T, Aoyama H, Nishimura T, Iguchi M, Hendrasto M (2017) Volcanic eruption volume flux estimations from very long period infrasound signals. Geophys Res Lett 44(1):143–151. https://doi.org/10.1002/2016GL071047

Yamada T, Aoyama H, Ueda H (2018) Relationship between infrasound-derived and buoyancy-derived eruption plume volume estimates. Bull Volcanol. https://doi.org/10.1007/s00445-018-1244-y

Yamakawa K, Ichihara M, Ishii K, Aoyama H, Nishimura T, Ripepe M (2018) Azimuth estimations from a small aperture infrasonic array: test observations at Stromboli volcano Italy. Geophys Res Lett 45(17):8931–8938. https://doi.org/10.1029/2018GL078851

Yamasato H (1997) Quantitative analysis of pyroclastic flows using infrasonic and seismic data at Unzen volcano. Japan J Phys Earth 45(6):397–416. https://doi.org/10.4294/jpe1952.45.397

Yokoo A, Tameguri T, Iguchi M (2009) Swelling of a lava plug associated with a Vulcanian eruption at Sakurajima Volcano, Japan, as revealed by infrasound record: Case study of the eruption on January 2, 2007. Bull Volcanol 71(6):619–630. https://doi.org/10.1007/s00445-008-0247-5

Yukutake Y, Honda R, Harada M, Doke R, Saito T, Ueno T, Sakai S, Morita Y (2017) Analyzing the continuous volcanic tremors detected during the 2015 phreatic eruption of the Hakone volcano. Earth, Planets Space 69(1):164. https://doi.org/10.1186/s40623-017-0751-y

Yukutake Y, Ichihara M, Honda R (2018) Infrasonic wave accompanying a crack opening during the 2015 Hakone eruption. Earth Planets Space https://doi.org/10.1186/s40623-018-0820-x

Publisher's Note